Hindawi Publishing Corporation
Journal of Spectroscopy
Volume 2013, Article ID 810247, 6 pages
http://dx.doi.org/10.1155/2013/810247

Research Article

Study on Fracture Healing with Small-Splint-Fixation Therapy by Near-Infrared Raman Spectroscopy

Hao Huang,[1] Shangyuan Feng,[2] Weiwei Chen,[1] Yun Yu,[1] Duo Lin,[1] and Rong Chen[2]

[1] *College of Integrated Traditional Chinese and Western Medicine, Fujian University of Traditional Chinese Medicine, Fuzhou 350108, China*
[2] *Key Laboratory of Optoelectronic Science and Technology for Medicine of Ministry of Education and Fujian Provincial Key Laboratory for Photonics Technology, Fujian Normal University, Fuzhou 350007, China*

Correspondence should be addressed to Rong Chen; chenr@fjnu.edu.cn

Received 2 May 2012; Revised 22 July 2012; Accepted 26 July 2012

Academic Editor: Kong-Thon Tsen

In this study, near-infrared (NIR) Raman spectroscopy was explored to assess the incorporation of calcium hydroxyapatite (CHA ~960 cm^{-1}) and other biochemical substances during the recovery of rabbits with complete radial fractures treated with or without small splints. 24 rabbits were randomy divided into two groups, one treated with small-splint-fixation therapy and the other without any intervention. The rabbits were sacrificed at 7, 15, 23, and 30 days after surgery, and the surface layers of the calluses in the fracture healing site from control and treated groups were routinely prepared for Raman spectroscopy. The prominent Raman bands were observed, including minerals at 430, 590, 960, 1003, and 1071 cm^{-1}, protein at 856, 876, 1246, and 1667 cm^{-1}, and lipid at 1767 cm^{-1}. The carbonate-to-phosphate ratio (CO_3 to υ_1 PO_4) and the mineral-to-matrix ratio (υ_1 PO_4 to amide I) were calculated from these normalized Raman bands. Comparison of the υ_1 PO_4-to-amide I ratio for the control group with that of the treated group probably indicated that the small-splint-fixation therapy could be useful for the gradual mineralization of the collagen matrix during fracture healing.

1. Introduction

Bone is a special material integrating an organic matrix, principally type I collagen, and an inorganic component [1]. Bone healing is an extremely complex process in human body, which has been under extensive investigation for many years [2].

The fixation therapy is the important and basic method to treat the bone fracture, and it is the fundamental condition that the bone fracture canbe concrescent on time [3]. Among numerous fixation therapies, elastic fixation therapy is the most reasonable and efficient technique for bone healing because, in elastic fixation therapy, the micromovement in the fracture ends of the bone is permitted, which can accelerate formation and calcification of callus and can be effective in promoting healing [4, 5]. As an important elastic fixation therapy, small-splint-fixation therapy fits on the trend of the healing of the fracture [6], whose guiding idea is "dynamic and static combination, equal stress on bones and muscles, exterior and interior treatment, and collaboration between doctors and patients." Microscopic examination and imaging are the cardinal methods for the assessment of small-splint-fixation therapy in promoting bone healing of rabbits with complete radial fractures nowadays. However, the influence of small-splint-fixation therapy on bone healing is still vague. Although the macroscopic properties of bone have been extensively examined and are somewhat established, the early steps in its mineralization are not well understood.

Raman spectroscopy (RS) can provide fingerprinting type information on the structure and conformation of macromolecules such as proteins, nucleic acids, and lipids [7]. RS has drawn considerable attention due to its great potential for improving clinical diagnosis [8–10] and obtaining precise information on biochemical composition [11–15]. Several groups have already investigated the applications of laser Raman spectroscopy for bone and tooth chemistry studies [16–18].

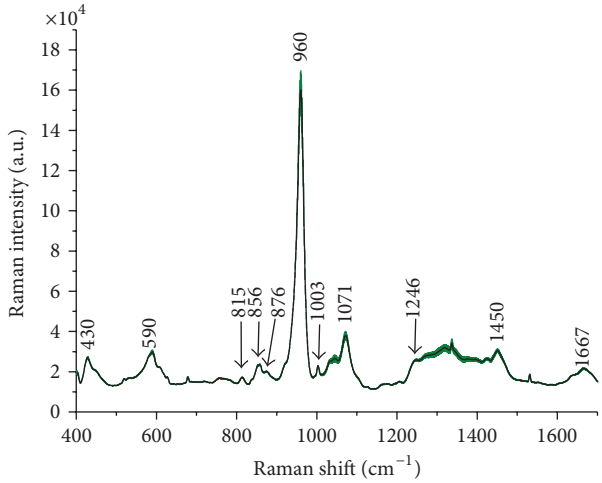

Figure 1: The mean Raman spectrum of the normal bone tissue sample. The shaded areas represent the standard deviations of the means.

Table 1: Raman peak position and vibrational mode assignment.

Peak positions (cm^{-1})	Major assignments
430	υ_2 vibration of phosphate
590	υ_4 vibration of phosphate
815	C–C stretch backbone
856	C–C stretch vibration of proline
876	C–C stretch of hydroxyproline
960	P–O symm. stretch (PO_4^{-3})
1003	phenylalanine ring breathing
1071	C–O in plane stretch (CO_3^{-2})
1246	C–N–H stretch of Amide III
1450	C–H bending mode of protein and lipid
1667	C–C–N stretch of amide I

During the bone fracture healing process, immature bone is replaced by a mature type of bone, which incorporates inorganic components with calcium hydroxyapatite (CHA, $Ca_{10}(PO_4)_6(OH)_2$) being the most important one. Similar to CHA, the level of bone mineral can characterize the presence of mineral on the bone; however, there may be other mineral phases present in the early stages of mineralization such as amorphous calcium phosphate and tricalcium phosphate. According to some researches, in less mineralized bone, there is a larger relative amount of monohydrogen phosphate and a smaller relative amount of carbonate. And the degree of mineralization will vary associated with bone development from the initial stages of formation to full maturity [19, 20].

In this study, NIR Raman spectroscopy was firstly used to investigate the effects of small-splint-fixation therapy on the healing of complete radial fractures in rabbits by monitoring the level of CHA at 7, 15, 23, and 30 days after surgery, using the P–O symmetric stretch band (960 cm^{-1}) as a prominent marker band. Moreover, carbonate-to-phosphate ratio and mineral-to-matrix ratio are also calculated from the normalized Raman band areas to obtain some useful information about bone components.

2. Materials and Methods

2.1. Experimental Animals and Model of the Bone Fracture. Twenty-four healthy adult male New Zealand rabbits (average weight at 2 kg) were purchased from Shanghai Laboratory Animal Center, Chinese Academy of Sciences (Laboratory animal use certificate no. SCXK (SH) 2007-0005) and raised in the Laboratory Animal Center of Fujian University of Traditional Chinese Medicine, qualified for specific pathogen free grade.

Under general anesthesia (xylazine hydrochloride injection 0.1 mL/kg (HuaMu, Jilin, China) and ketamine hydrochloride injection 0.1 mL/kg (Hengrui, Jiangsu, China)), the rabbits had their right legs shaved, and a 3 cm long incision was performed at the lower one-third part of radius with a n° 15 scalpel blade. Skin and subcutaneous tissues dissected down to periostea, which were gently sectioned so as to expose the bones. A 3 mm complete radial fracture was surgically produced as fracture healing model (low-speed drill, 1200 rpm, under refrigeration) in each rabbit [2]. All wounds were routinely sutured, and the rabbits received a single dose of benzylpenicillin sodium for injection (80.000 UI, Huaxing, Henan, China) immediately after surgery.

2.2. Randomization and Intervention Methods. After operation, the 24 rabbits were divided into two groups randomly by SPSS (Version 17.0) [21], including a control group ($n = 12$) and a small-splint-fixation treated group ($n = 12$). There was no internal or external fixation treatment for the control group. In the treated group, four pieces of small splints made by elastic fir tree barks are used in upper, lower, left, and right positions of the fractured leg, respectively, to fix the fracture bone well. Finally, small splints were tied up by bandage in order to prevent slippage.

2.3. Tissue Specimens Preparation. Three rabbits from each group were humanely killed at 7, 15, 23, and 30 days after the surgery with an overdose of general anesthetics, and the calluses from the fracture healing site were removed and longitudinally cut down to obtain the surface layer of the calluses as specimen by a Leica SP1600 saw microtome, which was specially designed for the cutting of extremely hard and brittle industrial materials. In order to minimize the growth of aerobic bacteria, the specimens were stored in liquid nitrogen, and the chemical fixation was not advisable as a result of the fluorescence emissions from the fixative substances. Prior to Raman study, without decalcified procedure, the specimens were warmed gradually to room temperature, washed by PBS, and then for Raman measurement.

2.4. NIR Raman Measurements and Data Processing. A confocal Raman microspectrometer (Renishaw, UK) with a 200 mW, 785 nm diode laser excitation was used for the

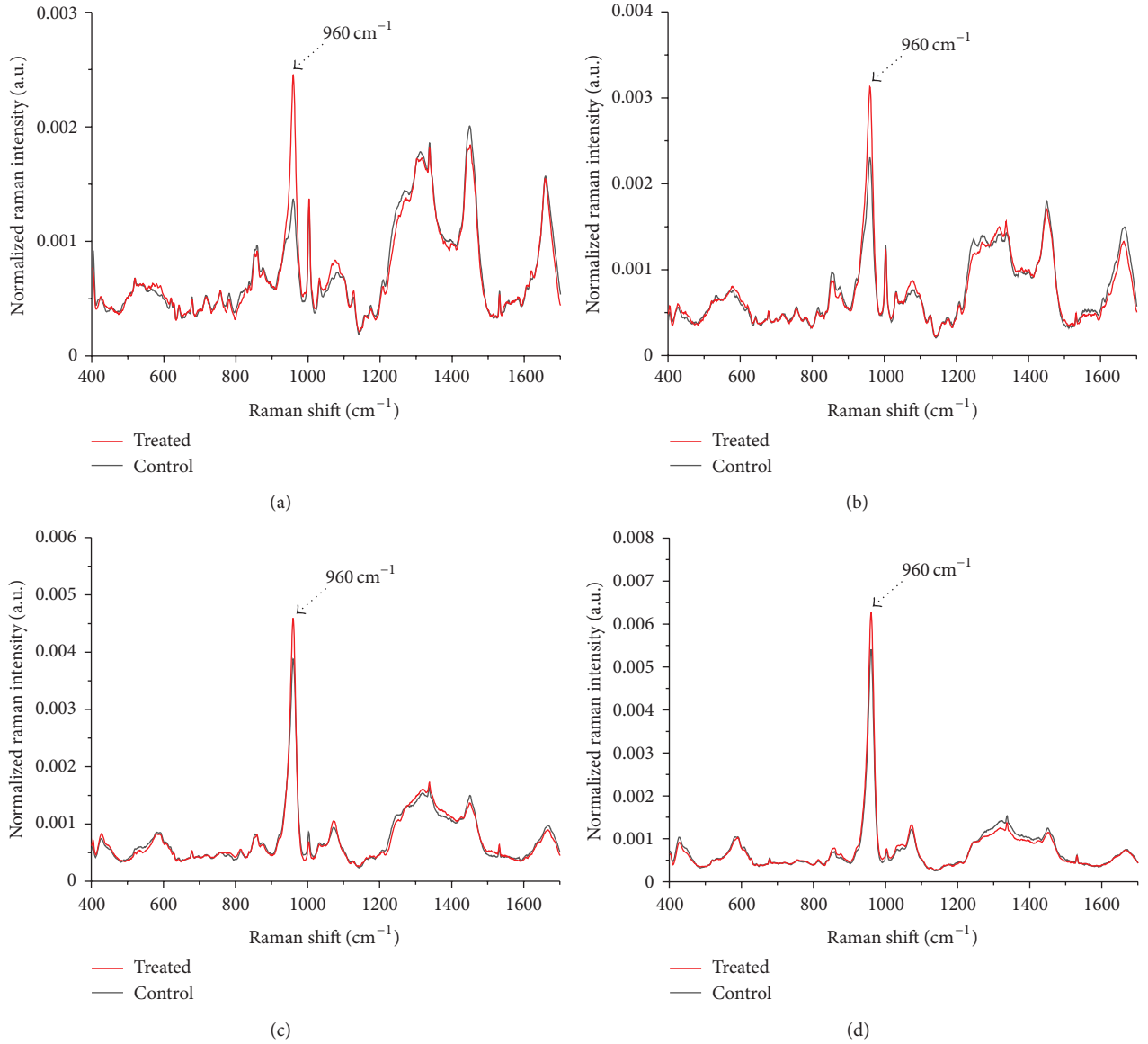

Figure 2: Mean normalized Raman spectra of the bones from control group and treated groups measured at (a) 7 days, (b) 15 days, (c) 23 days, and (d) 30 days after surgery.

measurement of Raman spectra. Briefly, all wavelength-calibrated spectra were corrected for the wavelength dependence of a standard 520 cm^{-1} vibrational band of a silicon wafer before Raman measurements and the software package WIRE 2.0 (Renishaw) was employed for spectral acquisition and analysis. The microscope was operated under a Leica 20× objective, which focused the laser beam onto a spot on the sample surface. For each sample, Raman measurements were performed on twenty random positions and two spectra were acquired from each position by repeated measurements. Therefore, in total forty Raman spectra were obtained from each sample. The signal was integrated for 10 s and measured over a spectral range of 400 to 1700 cm^{-1}.

The raw spectra of fracture healing sample acquired from control group and small-splint-fixation-treated groups in the 400–1700 cm^{-1} range represented a combination of prominent autofluorescence, weak Raman scattering signals, and noise. Thus, the raw spectra were preprocessed by adjacent five-point smoothing to reduce noise. And, then, an automated algorithm for autofluorescence background removal was applied to extract pure Raman spectra. The program was kindly offered by the BC Cancer Research Centre [22]. Then each of the background-subtracted Raman spectra was normalized to the integrated area under the curve from 400 to 1700 cm^{-1} to enable a better comparison of the spectral shapes and relative peak intensities among the different samples [7].

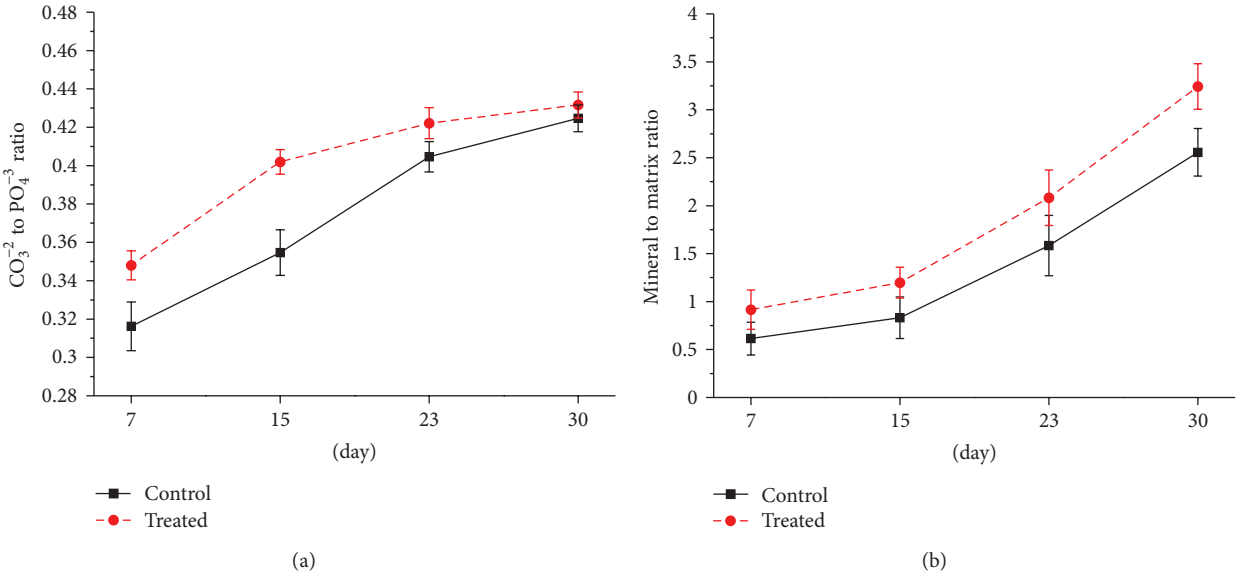

FIGURE 3: Scatter plot of the ratios of bone components measured as Raman band area ratios. (a) Carbonate-to-phosphate ratio (CO_3/υ_1PO_4); (b) mineral-to-matrix (υ_1PO_4/Amide I) ratio.

3. Results and Discussions

The fracture healing and bone strength are mainly affected by the organization of its mineralized collagen fibers and material composition. Important aspects of bone tissue quality include the physicochemical properties of its main constituents, the organic matrix, and the mineral crystals. Raman bands are sensitive to the distinction between structural and chemical changes in the compositional contribution of bone. Figure 1 shows the mean Raman spectrum of normal bone tissue. Prominent Raman bands are observed in the following peak positions with tentative biomolecular assignments: 430 cm^{-1} (υ_2 vibration of phosphate), 590 cm^{-1} (υ_4 vibration of phosphate), 960 cm^{-1} (P–O symmetric stretch vibration of hydroxyapatite), 1003 cm^{-1} (phenylalanine ring breathing), 1071 cm^{-1} (C–O in plane stretch vibration of carbonate hydroxyapatite), 1246 cm^{-1} (C–N–H stretch vibration of Amide III), 1450 cm^{-1} (C–H bending mode of protein and lipid), 1667 cm^{-1} (C–C–N stretch vibration of amide I), and so on. Table 1 lists tentative assignments for the observed Raman bands [1, 2, 17]. From Table 1, we could obtain that the molecular species of bone samples can be grouped into two principal components, the organic phase of the bone (proteins and lipid) and the inorganic (mineral) phase of the bone (phosphate, monohydrogen phosphate, and carbonate).

It was previously demonstrated that Raman band intensities depend strongly on both the chemical composition of the tissue and the fiber orientation with respect to the linear polarization direction of the exciting laser beam [23–25]. According to some literature data, biochemical composition and fiber orientation were determined from the following Raman bands: the phosphate (PO_4^{-3}), including υ_1PO_4 (integration area from 930 cm^{-1} to 980 cm^{-1}), the υ_2PO_4 (integration area from 410 cm^{-1} to 460 cm^{-1}), and υ_4PO_4 bending vibrations at 590 cm^{-1}, the amide I (integration area from 1620 cm^{-1} to 1700 cm^{-1}) and amide III (integration area from 1215 cm^{-1} to 1300 cm^{-1}), and the carbonate (CO_3^{-2}, integration area from 1050 cm^{-1} to 1100 cm^{-1}) [25].

The hydroxyapatite in bone mineral is characterized principally by the phosphate stretch (υ_1PO_4) spectral position, whose Raman band is at 960 cm^{-1}. Figure 2 shows the mean normalized Raman spectra of the surface layer of the calluses in the fracture healing site from control and treated groups at 7, 15, 23, and 30 days, respectively. As shown in Figures 2(a)–2(d), there was no significant shift in any band position throughout the data set; however, the constantly increasing intensity of 960 cm^{-1} peak was observed both in control and treated groups. As the 960 cm^{-1} band (phosphate υ_1PO_4) is a prominent marker for mineral content in bone, this result may indicate gradual mineralization during the fracture healing. Besides, the 960 cm^{-1} peak (υ_1PO_4) from the treated group shows higher percentage signals than that from the control groups in the same period of fracture recovering (7, 15, 23, and 30 days), probably indicating an increase in the percentage of hydroxyapatite content relative to the total Raman-active components in the treated group [1, 26, 27].

Although the Raman bands, such as υ_1PO_4 and amide I, are quite sensitive to the orientation and the polarization direction of the incident light, Raman bands such as amide III, υ_2PO_4, and υ_4PO_4 are less susceptible to the orientation effects [24, 25]. Therefore, Raman band areas obtained from the normalized curves were used to calculate several useful ratios of bone components. Carbonate is the most common substitution in the bone mineral lattice. The predominant substitution is type B carbonation (CO_3^{-2} replacing a PO_4^{-3}), containing a small amount of type A carbonation (CO_3^{-2} in place of OH^-) [1]. There is a strong band at 1071 cm^{-1}

indicating B-type carbonate substitution in the bone specimen. Figure 3(a) shows the ratio of the carbonate band at 1071 cm^{-1} to the phosphate band (υ_1PO_4, 960 cm^{-1}) between control group and treated group as a function of the time at 7, 15, 23, and 30 days after surgery. This ratio was calculated by dividing the integrated areas of the carbonate band (CO_3^{-2}, integration area from 1050 to 1100 cm^{-1}) and the phosphate band (υ_1PO_4, integration area from 930 cm^{-1} to 980 cm^{-1}), a recognized measure of mineral maturity [17]. As shown in Figure 3(a), a slight increase in the carbonate-to-phosphate ratio (CO_3^{-2}/PO_4^{-3}) was observed both in control and treated groups during the experiment. In addition, Figure 3(a) also shows that the carbonate-to-phosphate ratio of the treated group is higher than that of the control group at the same healing time. The maturation of the mineral in bone is indicated by the changes in the phosphate and carbonate modes. This change of carbonate-to-phosphate ratio is consistent with some studies such as bone tissue maturation [28] and mineralization of developing bone [29]. Meanwhile, this result indicated that an increase in carbonate occurs with increasing mineralization in bone tissue [1].

Figure 3(b) shows the variation of the mineral-to-matrix ratio between control group and treated group during the fracture healing. The mineral-to-matrix ratio, one of the most useful measurements for Raman analysis of bone, has been shown to be a marker of bone mineralization [17]. The mineral-to-matrix ratio was obtained from the integrated areas of any of the phosphate and amide peaks, which depend on both tissue organization and composition [24, 25]. This ratio was calculated by dividing the area of the phosphate band (υ_1PO_4, integration area from 930 cm^{-1} to 980 cm^{-1}) and the amide I band (integration area from 1620 cm^{-1} to 1700 cm^{-1}) [17]. As shown in Figure 3(b), the increase of the υ_1PO_4/amide I ratio occurs both in control group and treated group during the progress of fracture healing, which indicates the degree of mineralization, and the change in mineral-to-collagen ratio [23]. Figure 3(b) also shows that the treated group retained higher mineral-to-matrix ratio compared with the control group. This result probably indicated that the small-splint-fixation therapy could be useful for the gradual mineralization of the collagen matrix during fracture healing.

4. Conclusions

High-quality Raman spectra in the 400–1700 cm^{-1} range from rabbit bone tissue specimens in vitro were obtained by NIR Raman measurements. The prominent Raman peaks, such as 430, 590, 856, 876, 960, 1003, 1071, 1246, 1450, 1667, and 1767 cm^{-1} corresponding to biomolecules in bone tissue, were detected. These bands represented two principal components of bone tissue, including the organic components and the minerals. The promotion of fracture healing interfered by small-splint-fixation therapy was accessed by the analysis of phosphate band (υ_1PO_4, 960 cm^{-1}) during the experiment, which was a prominent marker for mineral content in bone. Other phosphate and carbonate vibrations could show the subtle changes in mineral composition, and the amide I and amide III could be used as typical markers in organic composition. The mineral-to-matrix ratio compared between the control group and the treated group probably indicated that the small-splint-fixation therapy could be useful for the gradual mineralization of the collagen matrix during fracture healing.

Acknowledgments

This work was supported by the National Natural Science Foundation of China (no. 61178090), the Project of the Educational Office of Fujian Province (no. JA10171), and the Developmental Fund of CHEN Ke-ji Integrative Medicine (no. CKJ2011010).

References

[1] M. D. Morris, S. Stewart, C. P. Tarnowski et al., "Early mineralization of normal and pathologic calvaria as revealed by Raman spectroscopy," in *Biomedical Vibrational Spectroscopy II*, vol. 4614 of *Proceedings of SPIE*, pp. 28–39, January 2002.

[2] C. B. Lopes, M. T. T. Pacheco, L. Silveira Jr., J. Duarte, M. C. T. Cangussú, and A. L. B. Pinheiro, "The effect of the association of NIR laser therapy BMPs, and guided bone regeneration on tibial fractures treated with wire osteosynthesis: Raman spectroscopy study," *Journal of Photochemistry and Photobiology B*, vol. 89, no. 2-3, pp. 125–130, 2007.

[3] R. Musharrafieh, O. Osmani, S. Saghieh, B. El-Hassan, and B. Atiyeh, "Microvascular composite tissue transfer for the management of type IIIB and IIIC fractures of the distal leg and compound foot fractures," *Journal of Reconstructive Microsurgery*, vol. 15, no. 7, pp. 501–508, 1999.

[4] C. J. Kershaw, J. L. Cunningham, and J. Kenwright, "Tibial external fixation, weight bearing, and fracture movement," *Clinical Orthopaedics and Related Research*, no. 293, pp. 28–36, 1993.

[5] B. Kassis, C. Glorion, W. Tabib, O. Blanchard, and J. C. Pouliquen, "Callus response to micromovement after elongation in the rabbit," *Journal of Pediatric Orthopaedics*, vol. 16, no. 4, pp. 480–483, 1996.

[6] A. Sarmiento, H. A. McKellop, A. Llinas et al., "Effect of loading and fracture motions on diaphyseal tibial fractures," *Journal of Orthopaedic Research*, vol. 14, no. 1, pp. 80–84, 1996.

[7] S. Feng, R. Chen, J. Lin et al., "Nasopharyngeal cancer detection based on blood plasma surface-enhanced Raman spectroscopy and multivariate analysis," *Biosensors and Bioelectronics*, vol. 25, no. 11, pp. 2414–2419, 2010.

[8] J. Lin, R. Chen, S. Feng et al., "Surface-enhanced Raman scattering spectroscopy for potential noninvasive nasopharyngeal cancer detection," *Journal of Raman Spectroscopy*, vol. 43, no. 4, pp. 497–502, 2012.

[9] S. Feng, J. Lin, M. Cheng et al., "Gold nanoparticle based surface-enhanced raman scattering spectroscopy of cancerous and normal nasopharyngeal tissues under near-infrared laser excitation," *Applied Spectroscopy*, vol. 63, pp. 1089–1094, 2009.

[10] J. Lin, R. Chen, S. Feng et al., "A novel blood plasma analysis technique combining membrane electrophoresis with silver nanoparticle-based SERS spectroscopy for potential applications in noninvasive cancer detection," *Nanomedicine*, vol. 7, no. 5, pp. 655–663, 2011.

[11] D. Lin, J. Lin, Y. Wu et al., "Investigation on the interactions of lymphoma cells with paclitaxel by Raman spectroscopy," *Spectroscopy*, vol. 25, no. 1, pp. 23–32, 2011.

[12] J. Lin, R. Chen, S. Feng et al., "Rapid delivery of silver nanoparticles into living cells by electroporation for surface-enhanced Raman spectroscopy," *Biosensors and Bioelectronics*, vol. 25, no. 2, pp. 388–394, 2009.

[13] Y. Yu, J. Lin, Y. Wu et al., "Optimizing electroporation assisted silver nanoparticle delivery into living C666 cells for surface-enhanced Raman spectroscopy," *Spectroscopy*, vol. 25, no. 1, pp. 13–21, 2011.

[14] H. Huang, W. Chen, J. Pan et al., "SERS spectra of a single nasopharyngeal carcinoma cell based on intracellularly grown and passive uptake Au nanoparticles," *Spectroscopy*, vol. 26, pp. 187–194, 2011.

[15] J. Lin, Y. Yu, B. Li et al., "Electrical pulse—mediated enhanced delivery of silver nanoparticles into living suspension cells for surface enhanced Raman spectroscopy," *Laser Physics Letters*, pp. 240–246, 2012.

[16] G. Penel, C. Delfosse, M. Descamps, and G. Leroy, "Composition of bone and apatitic biomaterials as revealed by intravital Raman microspectroscopy," *Bone*, vol. 36, no. 5, pp. 893–901, 2005.

[17] J. A. Timlin, A. Carden, and M. D. Morris, "Chemical microstructure of cortical bone probed by Raman transects," *Applied Spectroscopy*, vol. 53, no. 11, pp. 1429–1435, 1999.

[18] S. R. Goodyear, I. R. Gibson, J. M. S. Skakle, R. P. K. Wells, and R. M. Aspden, "A comparison of cortical and trabecular bone from C57 Black 6 mice using Raman spectroscopy," *Bone*, vol. 44, no. 5, pp. 899–907, 2009.

[19] H. E. Feki, C. Rey, and M. Vignoles, "Carbonate ions in apatites: Infrared investigations in the $\nu 4$ CO3 domain," *Calcified Tissue International*, vol. 49, no. 4, pp. 269–274, 1991.

[20] C. Rey, M. Shimizu, B. Collins, and M. J. Glimcher, "Resolution-enhanced fourier transform infrared spectroscopy study of the environment of phosphate ions in the early deposits of a solid phase of calcium-phosphate in bone and enamel, and their evolution with age. I: Investigations in the $\nu 4$ PO_4 domain," *Calcified Tissue International*, vol. 46, no. 6, pp. 384–394, 1990.

[21] V. Blankenship, C. M. Vega, E. Ramos et al., "Using the multifaceted Rasch model to improve the TAT/PSE measure of need for achievement," *Journal of Personality Assessment*, vol. 86, no. 1, pp. 100–114, 2006.

[22] J. Zhao, H. Lui, D. I. McLean, and H. Zeng, "Automated autofluorescence background subtraction algorithm for biomedical Raman spectroscopy," *Applied Spectroscopy*, vol. 61, pp. 1225–1232, 2007.

[23] M. Kazanci, H. D. Wagner, N. I. Manjubala et al., "Raman imaging of two orthogonal planes within cortical bone," *Bone*, vol. 41, no. 3, pp. 456–461, 2007.

[24] G. Falgayrac, S. Facq, G. Leroy, B. Cortet, and G. Penel, "New method for raman investigation of the orientation of collagen fibrils and crystallites in the haversian system of bone," *Applied Spectroscopy*, vol. 64, no. 7, pp. 775–780, 2010.

[25] S. Gamsjaeger, A. Masic, P. Roschger et al., "Cortical bone composition and orientation as a function of animal and tissue age in mice by Raman spectroscopy," *Bone*, vol. 47, no. 2, pp. 392–399, 2010.

[26] D. Lin, S. Feng, J. Pan et al., "Colorectal cancer detection by gold nanoparticle based surface-enhanced Raman spectroscopy of blood serum and statistical analysis," *Optics Express*, vol. 19, no. 14, pp. 13565–13577, 2011.

[27] S. Feng, R. Chen, J. Lin et al., "Gastric cancer detection based on blood plasma surface-enhanced Raman spectroscopy excited by polarized laser light," *Biosensors and Bioelectronics*, vol. 26, no. 7, pp. 3167–3174, 2011.

[28] H. J. Kim, J. H. Healey, C. D. Morris, and P. J. Boland, "Site-dependent replacement or internal fixation for postradiation femur fractures after soft tissue sarcoma resection," *Clinical Orthopaedics and Related Research*, vol. 468, no. 11, pp. 3035–3040, 2010.

[29] C. P. Tarnowski, M. A. Ignelzi Jr., and M. D. Morris, "Mineralization of developing mouse calvaria as revealed by raman microspectroscopy," *Journal of Bone and Mineral Research*, vol. 17, no. 6, pp. 1118–1126, 2002.